IOPscience iopscience.iop.org

Home Search Collections Journals About Contact us My IOPscience

Commensurability oscillations in a lateral superlattice with broken inversion symmetry

This content has been downloaded from IOPscience. Please scroll down to see the full text.

2015 New J. Phys. 17 043035

(http://iopscience.iop.org/1367-2630/17/4/043035)

View the table of contents for this issue, or go to the journal homepage for more

Download details:

IP Address: 132.199.100.37
This content was downloaded on 30/04/2015 at 09:23

Please note that terms and conditions apply.

New Journal of Physics
The open access journal at the forefront of physics

Deutsche Physikalische Gesellschaft DPG
IOP Institute of Physics

Published in partnership with: Deutsche Physikalische Gesellschaft and the Institute of Physics

OPEN ACCESS

RECEIVED
30 December 2014

REVISED
3 March 2015

ACCEPTED FOR PUBLICATION
18 March 2015

PUBLISHED
17 April 2015

Content from this work may be used under the terms of the Creative Commons Attribution 3.0 licence.

Any further distribution of this work must maintain attribution to the author(s) and the title of the work, journal citation and DOI.

PAPER

Commensurability oscillations in a lateral superlattice with broken inversion symmetry

M Staab[1], M Matuschek[1], P Pereyra[1], M Utz[1], D Schuh[1], D Bougeard[1], R R Gerhardts[2] and D Weiss[1]

[1] Experimentelle und Angewandte Physik, Universität Regensburg, D-93040 Regensburg, Germany
[2] Max-Planck-Institut für Festkörperforschung, Heisenbergstrasse 1, D-70569 Stuttgart, Germany

E-mail: dieter.weiss@ur.de

Keywords: magnetotransport, two-dimensional electron systems, lateral superlattice, Weiss oscillations

Abstract

We investigate both, experimentally and theoretically, commensurability oscillations in the low-field magnetoresistance of lateral superlattices with broken inversion symmetry. We find that pronounced minima develop in the resistivity ρ_{xx} when the flat band conditions of several relevant harmonics of the periodic potential nearly coincide.

1. Introduction

A unidirectional periodic potential $V(x)$, superimposed on a high-mobility two-dimensional electron system (2DES) constitutes a lateral superlattice (LSL), intensively investigated over the last decades (see [1] and references therein). In the presence of a perpendicular magnetic field B and for the electron mean free path l_e much longer than the potentials's period A, pronounced $1/B$ periodic commensurability oscillations (COs), also called Weiss oscillations, appear and reflect the interplay of the cyclotron radius $R_C = \hbar\sqrt{2\pi n_s}/(eB)$ at the Fermi energy E_F and the period A of the superlattice [2, 3]. Here, n_s is the carrier density of the 2DES. Minima in the resistivity ρ_{xx} appear in the case of a pure electrostatic modulation always then when

$$2R_C/A = (\lambda - 1/4) \tag{1}$$

holds. Here, $\lambda = 1, 2, 3$ .. is an integer. For magnetic field values fulfilling equation (1) the Landau levels become flat (flat-band condition), i.e. have no dispersion with respect to the wave vector k_y [3–5]. For flat Landau bands E_n with Landau index n the electron drift velocity $\propto \mathrm{d}E_n/\mathrm{d}k_y$ parallel to the grating disappears [3–5]. Within a fully classical picture the drift velocity resulting from classical $E \times B$ drift drops to zero if the average electric field probed by an electron on a cyclotron orbit vanishes [6]. Recently, it was shown, both experimentally [7–9] and theoretically [10–13] that LSLs with broken inversion symmetry can behave as a ratchet when illuminated by light [8–13] or when the potential barriers of the superlattice are driven by an ac potential [7]. A peculiar type of superlattice structure which guarantees inversion asymmetry consists of a periodic grating where the stripes inside a unit cell are separated by varying distances [9, 12, 13]. Figure 1(a) shows a corresponding arrangement of a nanopatterned gate on top of a high-mobility two-dimensional electron gas. The arrangement of the grating with three stripes of width a forming one unit cell is displayed in figure 1(b). Due to the different distances between the gate fingers and thus of the potential extrema it is *a priori* unclear what type of oscillatory features dominate the low-field magnetoresistance where the grating stripe separation and the cyclotron orbit are commensurate. Here we investigate, both experimentally and theoretically, the magnetotransport properties of LSLs with broken inversion symmetry and show that pronounced features in ρ_{xx}, i.e. minima, occur when the flat-band conditions for the dominating Fourier components of the superlattice nearly coincide. We note that a superlattice potential with broken inversion symmetry is only one example of a complex periodic potential composed of several different harmonics of different amplitude. While we focus here on a particular type of superlattice we also wish to stress that the theoretical framework used below can be applied to any other inharmonic superlattice potential.

© 2015 IOP Publishing Ltd and Deutsche Physikalische Gesellschaft

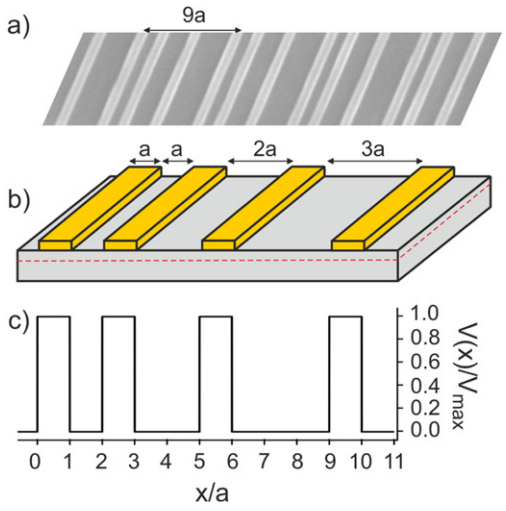

Figure 1. (a) Electron micrograph showing the superlattice grating on top of the GaAs/AlGaAs heterojunction. $a = 100$ nm. (b) Schematics of the grating with lacking inversion symmetry. The unit cell of the array contains three strips of width a. The distance between the centers of strip one and two is $2a$, that between the centers of strip two and three is $3a$, and that between the centers of strip three and the first one of the next unit cell is $4a$. Thus the width of the unit cell, i.e. the period of the array is $A = 9a$. (c) Model potential used in the calculations, lacking a point along the x-axis which could be a center of inversion and leave the superlattice potential invariant under point reflection at that point

2. Experiments

The superlattices were made from GaAs–AlGaAs heterojunctions having the 2DES 90 nm below the GaAs surface. Electron density and mobility of the unpatterned sample are at 4.2 K, $n_s \sim 2.2 \times 10^{11}$ cm^{-2} and $\mu \sim 9.2 \times 10^5$ cm^2 V^{-1} s^{-1}, respectively. Hall bars with a width of 50 μm and a separation of the potential probes of 40 μm have been fabricated by optical lithography and wet etching. Ohmic contacts are made of alloyed AuGe. The modulation of the carrier density has been achieved by depositing metallic stripes (AuPd on top of a thin layer of Ti) on the heterojunction surface. The stripes having a width of $a = 70$, 100 and 130 nm with an spacing of a, $2a$ and $3a$ within one unit cell (see figure 1(b)) were defined by electron beam lithography. In experiment the stripes were connected and grounded. The period A for the three different LSLs is thus $A = 630$, 900, and 1170 nm, respectively. Additionally, devices with symmetrically arranged stripes were also fabricated as a reference. The magnetoresistance was measured in a superconducting magnet system at 4.2 K using a low frequency ac current (typical amplitude of 100 nA) and lock-in detection. The magnetic field B was always applied perpendicular to the 2DES.

Figure 2 compares the low-field magnetoresistance ρ_{xx} of a LSL with inversion symmetric and asymmetric stripe arrangement. Both samples show a positive magnetoresistance around $B = 0$ which stems from open orbits parallel to the grating [14]. The oscillatory features which are in the focus of the present work are superimposed on a negative magnetoresistance at higher B. The period A of the symmetric device was 300 nm achieved by depositing 150 nm wide stripes separated by 150 nm. ρ_{xx} of the corresponding device shows the usual $1/B$ periodic oscillations described by equation (1). Also the sample with broken inversion symmetry with $a = 100$ nm and $A = 9a = 900$ nm shows oscillations, however with different spacing: the distinct minimum at about 0.18 T is surrounded by two less pronounced minima. It is also evident that the depths of the ρ_{xx} minima do not, in contrast to the symmetric grating, grow monotonously with increasing B. Figure 3 displays ρ_{xx} of three devices with inversion asymmetric LSL and different periods $A = 1170$, 900 and 630 nm. Also in these samples, a positive magnetoresistance prevails around $B = 0$ which is weakest in the sample with the smallest period. Since the depth of the 2DES is for all the samples 90 nm, the modulation amplitude is expected to be smallest in the sample with the smallest period. The pronounced ρ_{xx} minimum discussed for the 900 nm period sample above, shifts with increasing (decreasing) period A to smaller (larger) B-values. The carrier density of the different devices is within 10% the same and the different zero field resistivities reflect slightly different mobilities, also affected by the superimposed superlattice potential. As we will point out below the dominating ρ_{xx} minima in figures 3(a)–(c) occur when the flat-band conditions of the different Fourier components of the LSL potential coincide in a sufficiently narrow B-field interval. Due to different work function differences in gated and ungated regions, and different coefficients of expansion of the grating material and the underlying semiconductor [15, 16], the metal grating is connected with a lateral variation of the potential in the 2DES.

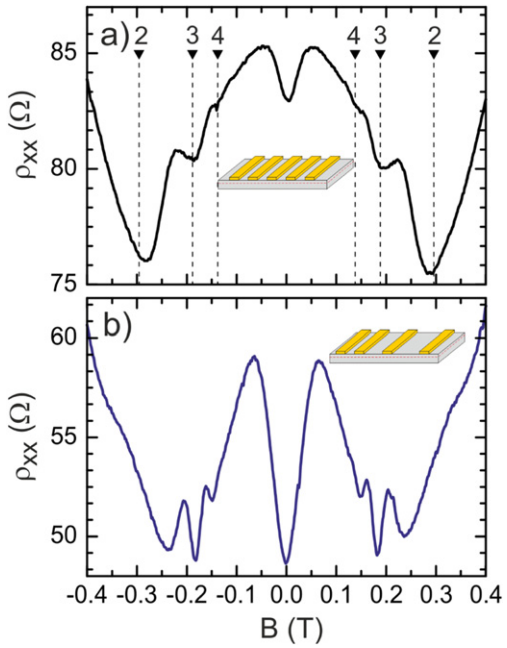

Figure 2. (a) Low-field magnetoresistance of a symmetric lateral superlattice with period $A = 300$ nm. The commensurability oscillations, superimposed on a negative magnetoresistance, show the usual sequence of minima described by equation (1), marked by dashed lines and the oscillation index λ. (b) Low-field ρ_{xx} for a LSL with broken inversion symmetry and period $A = 900$ nm. One of the unit cells contains three stripes of width 100 nm. Oscillation minima positions do not follow equation (1) and will be discussed in the text.

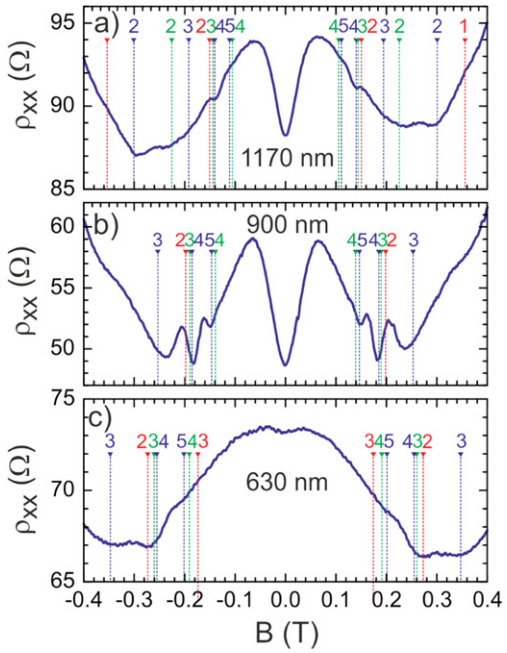

Figure 3. Comparison of the commensurability features for (a) 1170 nm, (b) 900 nm and (c) 630 nm. Triangles and dashed lines mark the flat band condition of different harmonics, discussed in the text. Different colors stand for different harmonics k (red = 2, green = 3, blue = 4) while the numbers correspond to the oscillation index λ. The color code is the same one as used in figures 5 and 6.

3. Theoretical description

For the theoretical description of the modulation we assume that the modulation effect of the metallic stripes on the surface can be adequately described by an electrostatic potential, and that we can neglect possible strain effects, on which we will comment below. We further assume that the modulation potential is weak enough, so that the contributions of its relevant Fourier coefficients to the resistance correction simply add [17]. To model

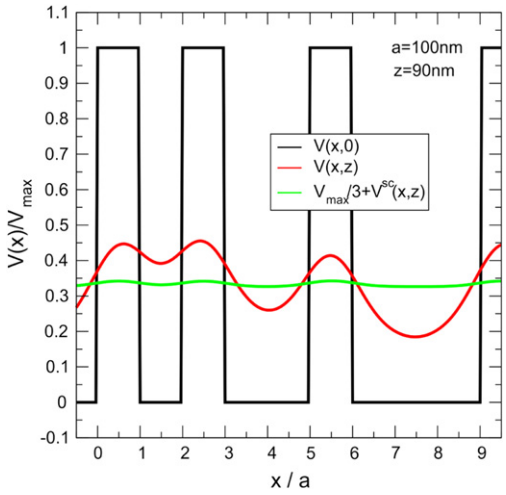

Figure 4. Model potential in the surface ($z = 0$, black) and corresponding potentials in the plane of the 2DES ($z = 90$ nm), without (red) and with (green) Lindhard screening. The potentials have period $9a$ and no inversion symmetry.

the effect of the inversion-asymmetric grating we assume that the grating induces in the surface plane $z = 0$ a periodic step potential of period $A = 9a$, which for $0 \leqslant x \leqslant A$ has the form

$$V(x) = V_{\max}\,[\theta(x)\theta(a - x) + \theta(x - 2a)\theta(3a - x) + \theta(x - 5a)\theta(6a - x)], \tag{2}$$

with $\theta(x)$ the Heaviside step function. This is a simplifying assumption, ignoring e.g. strain effects of the superlattice grating [16], but sufficient to understand the basic features observed in experiment. The corresponding superlattice potential is shown in figure 1(c). We also checked a different potential shape, namely Gaussians replacing the step functions, but the resulting differences between the two models are, due to electrostatic damping and screening (see below) not significant so that we focus on the simple rectangular potential shape. If the array of metal strips creates in the surface plane $z = 0$ the A-periodic potential

$$V(x, z = 0) = V(x) = V(x + A) = \sum_{k=-\infty}^{\infty} V_k \exp(\mathrm{i}kKx), \tag{3}$$

with $K = 2\pi/A$ and Fourier coefficients

$$V_k = \frac{1}{A}\int_0^A \mathrm{d}x\; V(x)\exp(-\mathrm{i}kKx), \tag{4}$$

and if there are no charges between the surface and the plane of the 2DES at a distance z, the Laplace equation requires an exponential damping of the Fourier components and leads to the effective potential [17]

$$V(x, z) = \sum_{k=-\infty}^{\infty} V_k(z)\exp(\mathrm{i}kKx) \tag{5}$$

with $V_k(z) = V_k \exp(-|k|Kz)$. The Fourier coefficients, equation (4), are $V_0 = V_{\max}/3$ and, for $|k| \gtrsim 1$, $V_k = V_{-k}^{\star} = (V_{\max}/2\pi k)(a_k + \mathrm{i}b_k)$ with

$$\begin{aligned} a_k &= \sin\xi + \sin 3\xi - \sin 2\xi + \sin 6\xi - \sin 5\xi, \\ b_k &= \cos\xi - 1 + \cos 3\xi - \cos 2\xi + \cos 6\xi - \cos 5\xi, \end{aligned} \tag{6}$$

where $\xi = kKa = 2\pi k/9$. The periodic potential in the plane of the 2DES will lead to a modulation of the electron density and, thereby, to a screening of the potential. In the regime of low magnetic fields, in which we are interested here, the linear screening approximation is sufficient. In this approximation the Fourier coefficient $V_k(z)$ of the external potential, equation (5), is reduced by the Lindhard dielectric constant $\varepsilon(q) = 1 + 2/(|q|a_B)$ of the 2DES to the screened form $V_k^{\mathrm{sc}}(z) = V_k(z)/\varepsilon(kK)$, with $a_B = 9.79$ nm the effective Bohr radius of GaAs [17, 18]. Based on the expressions given above the potential can be calculated numerically. For the width $a = 100$ nm and a distance $z = 90$ nm between surface and 2DES, the potentials in the surface and in the plane of the 2DES are shown in figure 4.

Within a semi-classical picture, appropriate at low magnetic fields at which Landau quantization and SdH-oscillations play no role, the correction to the resistivity can be written [17] as

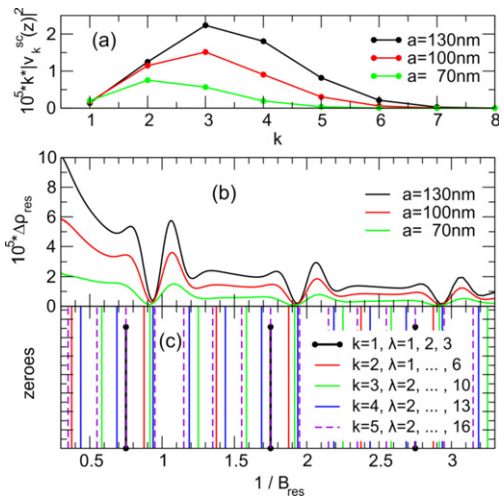

Figure 5. (a) Weight factors of the harmonics in equation (7) corresponding to the step potential with Lindhard screening. (b) $\Delta\rho_{xx}/\rho_0\eta$ as described by equation (7) with the weight factors of (a), as a function of $1/B_{\rm res}$. (c) Positions $1/B_{\rm res}\ (k,\ \lambda) = (\lambda - 1/4)/k$ of the zeros of the harmonic contribution to (b), see equation (7), for k = 1–4.

$$\Delta\rho_{xx}^{cl}/\rho_0 = \eta\ B_{\rm res} \sum_{k=1}^{\infty} k\ |v_k^{\rm sc}(z)|^2\ \cos^2\left(\frac{\pi k}{B_{\rm res}} - \frac{\pi}{4}\right). \tag{7}$$

Here, $B_{\rm res} = A/2R_C$ is the dimensionless rescaled magnetic field, $v_k^{\rm sc}(z) = V_k^{\rm sc}(z)/V_{\rm max}$ and $\eta = (4\pi\tau V_{\rm max})^2/(\pi\hbar^2 A^2 n_s)$ with the momentum relaxation time τ. For a purely harmonic modulation (only k=1) the above result has been obtained by purely classical arguments [6] and describes the conventional COs. As pointed out above we expect pronounced ρ_{xx} minima only if the drift velocity parallel to the grating, induced by the periodic potential, vanishes for all relevant harmonics k at about the same magnetic field value, i.e., the cosine term in equation (7) has to vanish for the dominating harmonics k. The contribution of the kth Fourier component of the modulation potential should thus vanish, if the rescaled magnetic field satisfies

$$B_{\rm res} = A/2R_c = \frac{k}{\lambda - 1/4} =: B_{\rm res}\ (k,\ \lambda), \quad \text{for} \quad \lambda = 1,\ 2\ ,.... \tag{8}$$

In the experiment only a few low Fourier components k contribute while higher k's have negligible weight. The weight factors $k|v_k^{\rm sc}(z)^2|$ relevant for the step potential with Lindhard screening are shown in figure 5(a) for the three different periods. They result from the counteracting effects of the Laplace equation and Lindhard screening. The Laplace equation leads to an exponential damping of higher Fourier coefficients, and becomes more effective with increasing k and decreasing period A. This explains that k's larger than six play no role, and that the overall amplitude of the modulation becomes smaller with the smaller period A. Lindhard screening, on the other hand, suppresses mostly the low-k Fourier coefficients and becomes more effective with increasing period A. As a result, the most relevant contributions to the resistance correction come from $k = 2,\ 3$ for $A = 630$ nm, from $k = 2,\ 3,\ 4$ for $A = 900$ nm, and from $k = 2,\ 3,\ 4,\ 5$ for $A = 1170$ nm, and the magnitude of the correction decreases with decreasing A. The corresponding correction to the Drude resistivity, equation (7), is shown in figure 5(b) for the three periods $A = 1170$ nm, 900 nm and 630 nm as a function of the inverse rescaled magnetic field $B_{\rm res}$. At specific $1/B_{\rm res}$ values pronounced minima in $\Delta\rho_{xx}$ appear. The most distinct one is the one occuring at about $1/B_{\rm res} \sim 0.9$. Here, the zeros of the resistivity for the harmonics $(k,\ \lambda) = (2,\ 2),\ (3,\ 3),\ \ldots(k,\ k)$ are lying closely together on the $1/B_{\rm res}$ scale; this coincidence of the zeros of different harmonics, displayed in figure 5(c), is responsible for the pronounced minimum in the resistivity.

4. Discussion

The most pronounced minimum at about $1/B_{\rm res} \sim 0.9$ in figure 5(b) can be seen in all experimental ρ_{xx}-traces displayed in figure 3. The magnetic field positions at which the contributions of the aforementioned harmonics $(k,\ \lambda) = (2,\ 2),\ (3,\ 3),\ (4,\ 4)$ and $(5,\ 5)$ vanish are marked by the dashed lines labeled '234' (and '432') in figure 3; they coincide well with the dominating minima in experiment. Apart from the dominating minimum the samples with periods A = 1170 and 630 nm show faint oscillatory features, discussed later. Generally, the experiment shows less oscillatory structure than the model calculation shown in figure 5. This is not surprising

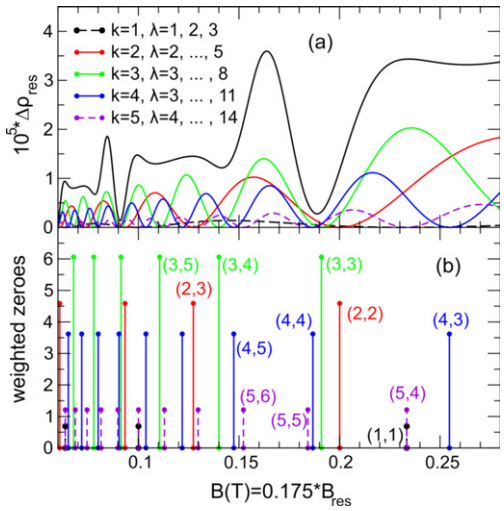

Figure 6. (a) Contributions of the individual harmonics for $k = 1, 2 \ldots, 5$ (colored lines) to the resistance correction and their sum $\Delta\rho_{res} = \Delta\rho_{xx}^{cl}/(\rho_0\eta)$, equation (7), (solid black line) versus magnetic field, for $n_s = 2.21 \times 10^{11}$ cm^{-2}, $A = 900$ nm, $z = 90$ nm. (b) The lines mark the position of the zeroes of the harmonics shown in (a), their lengths are proportional to the weights of the corresponding harmonics.

as scattering is taken into account in the model only by the momentum relaxation time τ taken from a homogeneous system.

Figure 5 also shows that the pronounced minima appear periodically on the $1/B_{res}$ scale. The second minimum at about $1/B_{res} \sim 1.95$ would occur for the 900 nm sample (see figure 3(b)) at about 0.088 T, where no visible structure is resolved anymore. This, on the other hand, means that the additional minima at $B \sim 0.15$ and 0.24 T, surrounding the dominant one of the 900 nm LSL at $B \sim \pm 0.18$ T in figure 3(b), do not stem from one of the dominating minima at which all relevant flat band conditions coincide. In order to get more insight into the origin of the oscillatory features we calculated the resistivity correction along the lines described above for the 900 nm LSL. The result is displayed in figure 6(a), showing the calculated $\Delta\rho_{xx}(B)$ for which five Fourier coefficients were taken into account. Also shown are the contributions of the individual Fourier components to the resistivity corrections, and, in figure 6(b), the zeroes of the harmonics specific for our step potential. The total resistivity correction shows, besides the pronounced minimum around $(k, \lambda) = (3, 3)$ two weaker minima at $B \sim 0.14$ and 0.26 T. These minima locations are close to the ones observed in experiment although they do not perfectly match. This is not surprising as the minima position depends on the relative weights of the involved Fourier contributions: the minimum at 0.26 T is dominated by the 4th harmonics (see blue trace in figure 6(a)) and the corresponding flat band condition (4,3), but the other Fourier contributions add up such that the minimum in the calculation is slightly shifted to higher field and significantly suppressed. Similarly for the minimum at about 0.14 T: it is close to the (3,4) and (4,5) flat band condition but the 2nd harmonics yields finite contributions.

The flat band conditions (4,3), (3,4) and (4,5) are also marked in figure 3(b). These minima positions agree quite well with the experimentally observed ones. The slight deviations from these marked positions depend on the weight of the involved Fourier coefficients and thus on the detailed shape of the superlattice potential. A shift of the relative weight will shift the minima positions. Using similar arguments we can assign the remaining features for the samples with $A = 1170$ and 630 nm. The 1170 nm superlattice displays a shoulder at about 0.10 T and additional local minima at about $B \sim 0.23$ and 0.29 T. As for the 900 nm period the shoulder can be assigned to the closely spaced flat band conditions for (3,4) and (4,5). The two minima at higher field match closely the flat bands for (3,2) and (4,2), indicated by the dashed lines in figure 3(a). The calculation, figure 5(b), yields for $A = 1170$ nm a relative minimum near the flat band condition (3,2), which is slightly shifted towards the nearby flat band position (4,3), whereas it yields no noticeable structure near (4,2). We now turn to the structure observed for the 630 nm superlattice in the low-field magnetoresistance. Since the modulation amplitude is smallest for the shortest period, only very weak oscillations are observed. Nonetheless, the minima positions correspond to the zeroes of the same harmonics as of the 900 nm sample, shown in figure 3(b). In the case of the 630 nm period sample we have in figure 3(c) also marked the (2,3) zeroes since the second Fourier component is the strongest for this period and is close to the (3,4) and (4,5) zeroes. It should be mentioned, though, that the minima corresponding to the zeroes of (4,3), (3,2) and (4,2) might be mimicked by the transition from a negative magnetoresistance to a positive, and therefore not connected to commensurability

features. The fact that the (4,3) minimum is absent in figure 3(a) points in this direction. Also the calculations show only weak structure in the vicinity of these zeroes.

In summary, we have shown that also in LSLs with broken inversion symmetry commensurability features emerge. To observe a minimum in the resistivity requires that flat band conditions of different harmonics nearly coincide, like (2,2), (3,3), (4,4) or (2,3), (3,4), and (4,5). Our analysis above is not only relevant for LSLs with broken inversion symmetry but generally for all types of LSL potentials where two or more Fourier components contribute to the resistivity correction. Another type of periodic surface modulation has been investigated by Endo and Iye [19], who deposited stripes of calixerene resist onto the surface, which caused a modulation due to strain effects. They considered, for instance, a simple periodic array of stripes and another array, in which they kept three neighboring stripes, then removed three stripes, and repeated this structure periodically. The low-temperature magnetoresistance of this 'hyperlattice' showed oscillations similar to the simple array. But the amplitude of the oscillations was smaller and, whereas most of the minima were close to those observed for the simple array, some minima were missing. We have checked that our approach can nicely reproduce this result, but only if we neglect the exponential damping required by the Poisson equation. If this modulation could be adequately described by an electrostatic surface potential, the sixth Fourier component of the hyperlattice potential, which corresponds to the period of the simple array, would be several orders of magnitude smaller than the lowest Fourier component, which would lead to a much larger period. The fact, that the magnetoresistance oscillation of the hyperlattice has a similar period as that of the simple lattice, indicates that the higher Fourier coefficients of the strain-induced modulation reach deeper into the sample than those of an electrostatic surface potential. From these results and the good agreement of experimental and theoretical results for the minima positions, which we obtained for the modulations with broken inversion symmetry, we conclude that there strain effects were indeed negligible.

References

[1] Gerhardts R R 1996 *Phys. Rev.* B **53** 11064
[2] Weiss D, von Klitzing K, Ploog K and Weimann G 1989 *Europhys. Lett.* **8** 179
[3] Gerhardts R R, Weiss D and von Klitzing K 1989 *Phys. Rev. Lett.* **62** 1173
[4] Winkler R W, Kotthaus J P and Ploog K 1989 *Phys. Rev. Lett.* **62** 1177
[5] Vasilopoulos P and Peeters F 1989 *Phys. Rev. Lett.* **63** 2120
[6] Beenakker C W J 1989 *Phys. Rev. Lett.* **62** 2020
[7] Hohberger E M, Lorke A, Wegscheider W and Bichler M 2001 *Appl. Phys. Lett.* **78** 2905
[8] Olbrich P, Ivchenko E L, Ravash R, Feil T, Danilov S D, Allerdings J, Weiss D, Schuh D, Wegscheider W and Ganichev S D 2009 *Phys. Rev. Lett.* **103** 090603
[9] Olbrich P, Karch J, Ivchenko E L, Kamann J, März B, Fehrenbacher M, Weiss D and Ganichev S D 2011 *Phys. Rev.* B **83** 165320
[10] Magarill L I 2001 *Physica E: Low-dimensional Syst. Nanostructures* **9** 652
[11] Ivchenko E and Ganichev S 2011 *JETP Lett.* **93** 673
[12] Popov V V, Fateev D V, Otsuji T, Meziani Y M, Coquillat D and Knap W 2011 *Appl. Phys. Lett.* **99** 243504
[13] Nalitov A V, Golub L E and Ivchenko E L 2012 *Phys. Rev.* B **86** 115301
[14] Beton P H, Alves E S, Main P C, Eaves L, Dellow M W, Henini M, Hughes O H, Beaumont S P and Wilkinson C D W 1990 *Phys. Rev.* B **42** 9229
[15] Davies J H and Larkin I A 1994 *Phys. Rev.* B **49** 4800
[16] Ye P D, Weiss D, Gerhardts R R, von Klitzing K, Eberl K, Nickel H and Foxon C T 1995 *Semicond. Sci. Technol.* **10** 715
[17] Gerhardts R R 1992 *Phys. Rev.* B **45** 3449
[18] Labbé J 1987 *Phys. Rev.* B **35** 1373
[19] Endo A and Iye Y 2000 *J. Phys. Soc. Japan* **69** 3656